Carbohydrate Polymers 101 (2014) 544–553

Contents lists available at ScienceDirect

Carbohydrate Polymers

journal homepage: www.elsevier.com/locate/carbpol

Understanding complex coacervation in serum albumin and pectin mixtures using a combination of the Boltzmann equation and Monte Carlo simulation

Yunqi Li, Qin Zhao, Qingrong Huang *

Department of Food Science, Rutgers University, 65 Dudley Road, New Brunswick, NJ 08901, USA

ARTICLE INFO

Article history:
Received 5 February 2013
Received in revised form
10 September 2013
Accepted 17 September 2013
Available online 25 September 2013

Keywords:
Turbidimetric titration
Monte Carlo simulation
Sigmoidal Boltzmann equation
Protein
Polysaccharide
Complex coacervation
Binding

ABSTRACT

A combination of turbidimetric titration, a sigmoidal Boltzmann equation approach and Monte Carlo simulation has been used to study the complex coacervation in serum albumin and pectin mixtures. The effects of the mass ratio of protein to polysaccharide on the critical pH values, the probability of complex coacervation and the electrostatic interaction from charge patches in serum albumin were investigated. Turbidimetric titration results showed an optimum pH for complex coacervation (pH_m), which corresponded to the maximum turbidity in the protein/polysaccharide mixture. The pH_m monotonically decreased as the ratio decreased, and could be fitted using the sigmoidal Boltzmann equation. It suggests that pH_m could be a good ordering parameter to characterize the phase behavior associated with protein/polysaccharide complex coacervation. Qualitative understanding of pH_m by taking into account the minimization of electrostatic interaction, as well as quantitative matching of pH_m according to the concept of charge neutralization were both achieved. Our results suggest that the serum albumin/pectin complexes were ultimately neutralized by the partial charges originated from the titratable residues in protein and polysaccharide chains at pH_m. The Monte Carlo simulation provided consistent phase boundaries for complex coacervation in the same system, and the intermolecular association strength was determined to be several k_BT below the given ionic strength. The strongest binding site in the protein is convergent to the largest positive charge patch if pure electrostatic interaction was considered. Further inclusion of contribution from excluded volume resulted in the binding site distribution over five different positive charge patches at different protein/polysaccharide ratios and pH values.

1. Introduction

Complex coacervation in protein and polysaccharide mixtures is an associative liquid–liquid phase separation. It has broad applications in microencapsulation, protein purification, and the stabilization of food emulsions etc (Dickinson, 2008; Liu, Low, & Nickerson, 2010; Xu, Mazzawi, Chen, Sun, & Dubin, 2011). Fundamental investigations of the complex coacervation in protein/polysaccharide mixtures from multi-length scales, including molecular interactions, binding, association of molecules and phase behaviors are critical not only for scientific research, but also for novel functional materials development.

Currently, various protein/polysaccharide mixtures have been used in food processing and products, pharmaceutical processing and controlled release etc., depending upon their chemical specificities, physical properties and biocompatibility (Dickinson, 2003). Understanding the interactions involved in the stabilization of protein/polysaccharide coacervate is not straightforward (Dickinson, 1998). The elementary interactions largely rely on extrinsic physicochemical conditions including temperature, pH, ionic strength, concentration, and protein/polysaccharide ratio etc., as well as the intrinsic characters of biomacromolecules such as charge density of polysaccharide chains and distribution of surface charge in proteins. The widely accepted major interaction contributed to complex coacervation is the electrostatic interaction (Gummel, Boue, Clemens, & Cousin, 2008) and sometimes the depletion force when neutral polysaccharide was included (Dickinson, 2008). Beyond the interactions, at tens of nanometer to micrometer scale, both the long range interaction network (association) and the steric stabilization (packing) play an important role during complex coacervation. A certain degree of packing and association strength is imperative to form visible phase domain, and to sustain the phase domain against thermo fluctuation. There are two limits in protein/polysaccharide mixtures (Bohidar, Dubin, Majhi, Tribet, & Jaeger, 2005): in the protein-rich mixture, polysaccharide chains were confined in a continuum of protein-rich domains; in

* Corresponding author. Tel.: +1 848 932 5514; fax: +1 732 932 6776.
E-mail address: qhuang@aesop.rutgers.edu (Q. Huang).

0144-8617/$ – see front matter © 2013 Elsevier Ltd. All rights reserved.
http://dx.doi.org/10.1016/j.carbpol.2013.09.056

polysaccharide-rich mixture, proteins were dispersed in transient meshes constructed by polysaccharide chains in semi-dilute solutions. Under these limits, complex coacervation may be inhibited because of non-neutralized charges when one of the biopolymers is in excess (Schmitt, Sanchez, Desobry-Banon, & Hardy, 1998). Systematic study of the complex coacervation of well-known proteins and polysaccharides using a combination of computation simulation and experiments is a good approach to understand how the molecular association and microstructure change with complex coacervation. Our recent work on complex coacervation of bovine serum albumin (BSA) and pectin (Ru, Wang, Lee, Ding, & Huang, 2012) indicated that phase boundary (the critical pH where global phase separation occurred) shifted with the initial composition of BSA and pectin. We continue to work on the same system from different angles to reveal the determinant which contributed to the phase behaviors associated with protein and polysaccharide complex coacervation.

BSA is a well-known model protein in complex coacervation study. Dubin and others have published a number of papers in the complex formation of BSA with poly(diallyldimethylammonium chloride) (PDADMAC)-based polyelectrolytes (Antonov, Mazzawi, & Dubin, 2010; Bohidar et al., 2005; Grymonpre, Staggemeier, Dubin, & Mattison, 2001; Kayitmazer, Strand, Tribet, Jaeger, & Dubin, 2007; Li, Mattison, Dubin, Havel, & Edwards, 1996; Seyrek, Dubin, Tribet, & Gamble, 2003; Xia, Dubin, & Dautzenberg, 1993; Xu et al., 2011). Phase boundaries, binding affinity and the structure in these complexes have been systematically investigated. They introduced the concept of charge patches, which were defined as a part of the protein providing strong binding to a given polyelectrolyte, to facilitate the understanding of binding "on the wrong side of p*I*", with p*I* the isoelectric point of a protein. As a classic model protein, BSA has been intensively studied, and the charge patch concept is extremely helpful in understanding the versatile capabilities of BSA to form complexes with various polyelectrolytes. For example, Laos et al. found that both BSA and β-lactoglobulin carried an average net charge of the same sign as the furcellaran when they formed complexes (Laos, Brownsey, & Ring, 2007). Recently, we used an alternative definition of charge patches, which consist of spatially neighbored titratable residues (i.e., solvent accessible and charged residues) of the same sign of charges. Our approach was inspired by the concept of binding sites in proteins which provide topological pocket to bind given molecules (Del Carpio, Takahashi, & Sasaki, 1993), also provided meaningful details of BSA complex coacervation with a polycation through Monte Carlo simulations (Li, Shi, Huang, & An, 2012). Furthermore, Chodankar, Aswal, Kohlbrecher, Vavrin, and Wagh (2008) studied the BSA/sodium polystyrene sulfonate (NaPSS) complexes using small-angle neutron scattering (SANS), and found equilibrium distributions of polyelectrolyte chains in saturated (charge neutralized) or free bound proteins as well as complexes in supernatants or in coacervates. BSA has also been studied in a wide range of food related areas including emulsion stability (Dickinson, 2003; Tolstoguzov, 2003), encapsulation and release (Burova et al., 1999; de Kruif, Weinbreck, & de Vries, 2004), surface adsorption (Brzozowska, de Keizer, Norde, Detrembleur, & Stuart, 2010; Brzozowska, Zhang, de Keizer, Norde, & Stuart, 2010; Wang, Ho, & Huang, 2007), multiple layer assemble for biosensors (Caruso & Mohwald, 1999), macro-encapsulation for scaffold development (Toh, Ho, Zhou, Hutmacher, & Yu, 2005) etc. Therefore, fundamental studies of the protein/polysaccharide complex coacervation in BSA solutions have broad impacts.

Pectin, a polysaccharide extracted from fruits, is traditionally used as a gelling agent. It has also received considerable attentions because of its capability to form complex coacervate. Jones et al. prepared nanoparticles with different structures and aggregation proneness using complex coacervates of β-lactoglobulin and pectin through different thermal treatments (Jones, Decker, & McClements, 2010). Schmidt et al. used SANS to study lysozyme/pectin complex, and found that increasing charges in pectin chains could enhance the packing of proteins (Schmidt, Cousin, Huchon, Boue, & Axelos, 2009). Bedie et al. studied the encapsulation of thiamine using whey protein isolate/pectin complexes, and found that the complexes had optimum entrapment efficiency at pH 3.5 (Bedie, Turgeon, & Makhlouf, 2008). Wang et al. have studied the effects of salt concentration and protein/polysaccharide ratios on the assembly, structure and rheological properties of β-lactoglobulin/pectin complexes (Wang, Wang, Ruengruglikit, & Huang, 2007; Wang, Lee, Wang, & Huang, 2007). Researches related to the complex coacervation using pectin and proteins were also found in several comprehensive reviews (Dickinson, 1998, 2003; Tolstoguzov, 2003). Although many researches related to pectin-based complex coacervation have been reported, thorough understanding of the role of pectin in the coacervation process is far from clear.

In this work, we used a combination of turbidimetric titration, and theoretical approaches particularly Monte Carlo simulation to study the complex coacervation in serum albumin/pectin mixtures. A set of turbidimetric titration experiments, and the Monte Carlo coarse grained model based on the specified charge distribution in serum albumin and polysaccharide (PS), pectin in this work were first described. Subsequently, we presented the effect of the mass ratios of protein/PS on titration curves and the optimum pH for complex coacervation. A tentative theoretical understanding of this effect by taking into account of energy minimization and charge neutralization was provided. In the simulation part, phase boundaries associated with percolation concepts and simulation configurations were determined and compared with experimental observation. The binding affinity of charge patches in protein and the structure in the mixtures were also thoroughly studied. Finally, findings obtained from this work and results related to the effects of protein/PS ratio on complex coacervation were also discussed in detail.

2. Materials and methods

2.1. Turbidimetric titration experiments

Bovine serum albumin (BSA) was purchased from Sigma Chemical Co. (Lot: 058K0726, St. Louis, MO). LM-Pectin with 31% esterification (Danisco A/S, Denmark) was purified by dialysis (MWCO = 12,000) followed by freeze-drying, similar to the procedure used in our previous works (Ru et al., 2012; Wang, Wang, et al., 2007; Wang, Lee, et al., 2007). Sodium chloride (NaCl), sodium hydroxide (NaOH) and hydrochloric acid (HCl) were purchased from Fisher Scientific (Pittsburgh, PA). All solutions for the titration experiments were prepared using Milli-Q water.

Solutions of BSA to pectin mass ratios (α) ranging from 9:1 to 1:9 were titrated whereas the total concentrations of BSA and pectin mixtures were kept at a constant of 3.0 mg/mL, and the salt (NaCl) concentration was fixed at 0.1 M. At this salt concentration, the small amount of ions released from either protein or polysaccharide became negligible. In the control titration of pure BSA or pectin saline solutions, the concentration of biopolymer was fixed at 2.5 mg/mL with the same salt concentration. The pH meter (Thomas Scientific 8025) was calibrated with two buffers of pH 4.0 and 7.0, respectively, and the turbidity detector (Brinkman PC 910 colorimeter equipped with a 1 cm path length optical probe and a 420 nm filter) was calibrated by Milli-Q water. The turbidity, which was defined as $(100 - 100 * I_1/I_0)\%$, was used to detect the aggregation and the phase separation in samples. Here I_0 and I_1 are the intensities of the incident and transmitted light, respectively. All solutions (except two solutions in control titrations which were

adjusted to pH 2.0 instead) were adjusted to pH 8.0 using 0.1 M NaOH, followed by filtering through 0.45 μm VWR syringe filters prior to titration. To minimize the dilution arising from titration, low concentration (0.1 M) and high concentration (6 M, only used when pH < 2.0) HCl solutions were used to adjust the pH of the mixtures under magnetic stirring. All titration experiments were carried out under ambient conditions, and samples were allowed to equilibrate for 5 min before a droplet of titrating solution was added to minimize kinetic perturbation during titration.

2.2. Monte Carlo simulation

2.2.1. Model

Serum albumin was modeled as a soft sphere with charge patches. The equivalent radius of the sphere is 30 Å (Bendedouch & Chen, 1983) which is a coarse-grained model based on the native structure of human serum albumin (HSA, PDBid: 1e7i). In all the 585 residues, 100 residues are potentially positive charged (R, K, H and N-term) and 116 residues are potentially negative charged (D, E, Y and C-term). The p*K* values of these ionizable residues were set according to a recent report (Pace, Grimsley, & Scholtz, 2009). By regarding the exposed residues assigned by DSSP (Kabsch & Sander, 1983), the 71 positive charged residues and 92 negative charged residues (i.e., titratable residues (Tanford & Kirkwood, 1957)) can be assembled into charge patches when the beta-carbons (C_β) in any two titratable residues (bring same sign of charges) approach to less than 12 Å. Such a cut-off was referred to the full structural fingerprint related to protein thermostability (Li & Fang, 2010), and the optimum cutoff for interface alignment-based docking algorithm design (Sinha, Kundrotas, & Vakser, 2012). The location of each patch, which was the geometrical center of all C_β atoms of residues in the patch (referred to the geometrical center of the protein), was recorded by internal coordinates. The size of each patch was tentatively set as one-third of the radius of gyration of these C_β atoms. The partial charge held brought with each residue was calculated according to acid-base equilibrium described in our recent work (Li et al., 2012). Finally, each charge patch was modeled by a hard sphere with the partial charge loaded in the center of the sphere. Finally, the coarse-grained model for serum albumin included a large soft sphere to represent the excluded volume of the protein, and hard spheres to present charge patches as illustrated in Fig. 1.

Pectin was modeled as a freely jointed chain (FJC) with a string of soft beads. Each bead represents a disaccharide segment with a radius of 5.0 Å (Marcelo, Saiz, & Tarazona, 2005; Marszalek, Li, Oberhauser, & Fernandez, 2002), and loads a partial charge derived from the dissociation of —COOH group. Though there may be some branches in the pectin sample used in this work, we still approximately model it as linear chain for simplicity. Solvent was implicitly modeled as a dielectric continuum in this work. It is worthy to note that in the simulation model, all charges are located in the center of hard spheres, which avoids zero-distance contact known as Manning condensation (Manning, 1969) during electrostatic interaction calculation.

2.2.2. Potential

The potential to guide the Monte Carlo simulation was defined as

$$U = \sum_{i,j} U_{\mathrm{VDW}}(i,j) + \sum_{i,j} [U_{\mathrm{ELE}}(i,j) + U_{\mathrm{HS}}(i,j)] \quad (1)$$

The first summation is computed from all protein–protein pairs, protein–bead pairs and bead–bead pairs, and the second summation is against all patch–patch pairs, patch–bead pairs and bead–bead pairs. The van der Waals potential is calculated through Lennard-Jones potential

$$U_{\mathrm{VDW}}(i,j) = \varepsilon_{ij}\left[\left(\frac{\sigma_{ij}}{r_{ij}}\right)^{12} - 2\left(\frac{\sigma_{ij}}{r_{ij}}\right)^{6}\right] \quad (2)$$

where r_{ij} is the distance between coarse-grained particles i and j, $\sigma_{ij} = (\sigma_i + \sigma_j)/2$ and $\varepsilon_{ij} = \sqrt{\varepsilon_i \varepsilon_j}$ with σ_i and ε_i (fixed at $1.0 k_B T$ in this work with k_B the Boltzmann constant) are the van der Waals radius and the potential well. The electrostatic potential (ELE) was calculated through Debye–Hückel approximation, i.e.

$$U_{\mathrm{ELE}}(i,j) = \lambda_B k_B T u_i u_j / r_{ij} \exp(-r_{ij}/\lambda_D) \quad (3)$$

Here u_i, u_j are the partial charges brought by charge patches and PS beads in electric charge unit, λ_B is the Bjerrum length which is 7 Å in water under ambient condition, λ_D is the screening length which equals 9.74 Å and corresponds to 0.1 M monovalent salt solution. The hard-sphere (HS) potential was defined as

$$U_{\mathrm{HS}}(i,j) = \begin{cases} +\infty, & \forall r_{ij} < (\sigma_i + \sigma_j)/2 \\ 0 & \text{otherwise} \end{cases} \quad (4)$$

It is only applicable for interactions involving charge patches, in order to avoid steric overlapping when strong electrostatic attraction overcomes van der Waals repulsion from the whole protein.

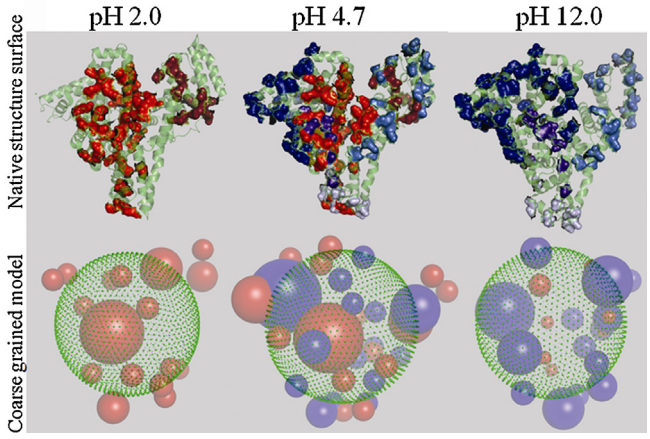

Fig. 1. The distribution of charge patches in serum albumin native structure (PDB: 1e7i) and in coarse grained protein model. Red based color shows the top largest positive charge patches, and from red to ruby the size of charge patch decreases; blue based color represents the top largest negative charge patches, from blue to gray the size of charge patch decreases. Each charge patch is represented by a hard sphere, and the green mesh represents the excluded volume of the whole protein. (For interpretation of the references to color in this figure legend, the reader is referred to the web version of the article.)

2.2.3. Simulation and complex identification

In Table S1 (see supplementary information) we presented the parameter settings used in the Monte Carlo simulation, and the simulation configuration updating and conformation sampling were described elsewhere (Li et al., 2012). In brief, the simulation was guided under Metropolis rule (Metropolis, Rosenbluth, Rosenbluth, Teller, & Teller, 1953), and a reasonable truncate of 18 Å for electrostatic potential calculation (Norberg & Nilsson, 2000) was adopted to speed up the simulation. To achieve configurations under thermodynamic equilibrium, we first evenly dispersed proteins and PS chains in a simulation box, followed by 6×10^5 MCS relaxation without electrostatic interaction to avoid artificially induced local enrichment of molecules. Here, each MCS represents the simulation time where all PS beads and proteins have one attempted movement on average. Then another 6×10^5 MCS simulation with all

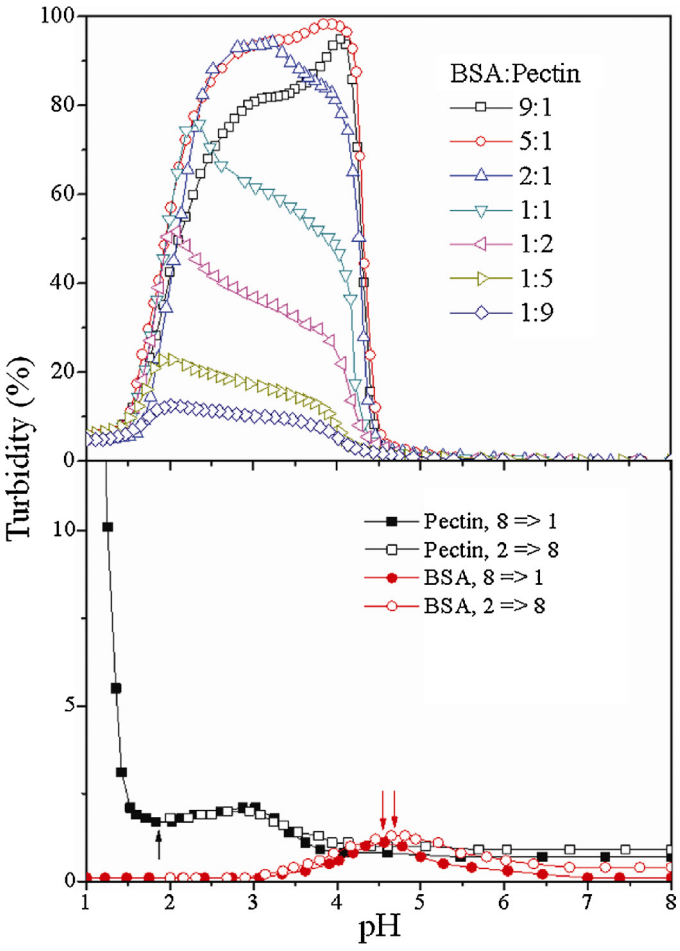

Fig. 2. Turbidimetric titration as a function of protein/polysaccharide ratio (top), and control titration of BSA and pectin saline solutions (bottom). The arrows label out the pH with maximum turbidity in control titration experiments. The NaCl concentration is fixed at 0.1 M.

energy terms was carried out starting from the final configuration after the first stage of simulation. Simulation configurations were recorded in every 10^4 MCS in each trajectory. Finally, we collected 100 configurations by taking the final 25 configurations from four parallel trajectories (different initial placements of molecules in simulation box and different random seeds during both stages of simulations) for the results presented below.

A complex or a complex coacervate is formed through intermolecular association. Two molecules are associated only if $U < \Gamma k_B T$. Here U is the intermolecular interaction which is the sum of all interaction pairs between two molecules according to Eq. (1). Γ is -1 representing random associations which can be disassociated by thermal fluctuation, and more negative standing for stronger association. A complex contains at least one PS chain and one protein, which further trapped more molecules to form coacervate once a geometric percolated aggregate was formed in a simulation configuration.

3. Results

3.1. Turbidimetric titration

The turbidimetric titrations of BSA/pectin mixtures at different ratios, and the control titration curves of BSA or pectin saline solutions were shown in Fig. 2. It can be seen that the pH window for the formation of complex and complex coacervate is almost unchanged against the protein/polysaccharide ratio (α). The maximum

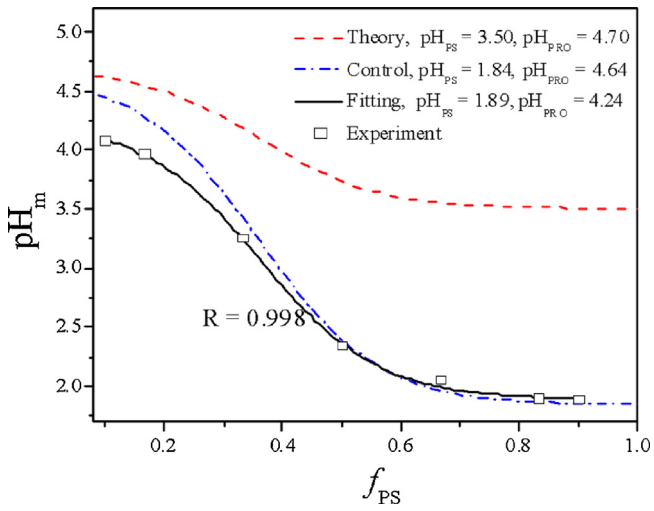

Fig. 3. The pH_m is plotted against the mass fraction of pectin and fitted by sigmoid Boltzmann equation with different thresholds. The NaCl concentration is fixed at 0.1 M.

turbidities are high when protein is in excess, and decrease when more PS chains replaced proteins. Most interestingly, the optimum pH where the turbidity reaches a maximum (named as pH_m) gradually shifts to lower pH values as α decreases. According to the control titration curves of pure BSA or pure pectin saline solutions, either titrated from pH 8.0 to pH 1.0 (labeled as 8 = >1 in Fig. 2) or in reverse direction (labeled as 2 = >8), we obtained the critical pH value for pure BSA saline solution at 4.64 (an average of the peak values at both curves), and 1.84 for pectin solution. The former critical pH may be referred as the p*I* of BSA, which was reported to be 4.70 (Ge, Kojio, Takahara, & Kajiyama, 1998; Li, Lee, Lal, An, & Huang, 2008). The latter is lower than the pK_a of pectin reported as 3.50 (Kalapathy & Proctor, 2001), instead, we selected the threshold corresponding to the initial aggregation of pectin chains trying to provide quantitative understanding of the critical pH values in the complex coacervation. The hysteresis shown in the control titration curves is almost negligible, which suggests the apparent shift of turbidity curves and the pH_m in BSA/pectin mixtures is originated not from the kinetics in the liquid–liquid associative phase separation (i.e., coacervation), but of thermodynamic factors.

3.2. Theoretical understanding of pH_m

It seems that pH_m brings abundant information toward the understanding of turbidity titration data. At first, we plotted pH_m values against the mass fraction of pectin, f_{PS} which can be directly calculated by $(1+\alpha)^{-1}$ and shown in Fig. 3. We then fitted the pH_m versus f_{PS} using sigmoid Boltzmann equation, which has been used to describe the gelation in polymer solutions (Li, Sun, Shi, & An, 2004; Li et al., 2007). The equation is written as

$$pH_m = pH_{PS}\left\{1 + \frac{pH_{PRO} - pH_{PS}}{pH_{PS}}\left[1 + \exp\left(\frac{f_{PS} - f_{PS,c}}{\Delta f_{PS}}\right)\right]^{-1}\right\} \quad (5)$$

In this equation, Δf_{PS} is a constant fitting parameter of 0.1, and $f_{PS,c}$ is a transition point: below it, pH_m has strong dependence on f_{PS}; above it, pH_m is almost independent on f_{PS}. The pH_{PRO} and pH_{PS} are the critical pHs where protein and polysaccharide may endure significant change in their properties. The best fit with a correlation coefficient of 0.998 provided pH_{PRO} and pH_{PS} of 4.24 and 1.89, and $f_{PS,c}$ got a value of 0.36 which corresponds to α value of 1.75:1. The predicted pH_m values using pH_{PRO} and pH_{PS} values according to the known critical values (4.70 and 3.50 for pH_{PRO}

and pH_{PS}, respectively), the control titration experiment (4.64 and 1.84) were also presented for comparison. The experimental results deviated from the curves generated from either the known critical values for protein and polysaccharide or the control titration measurements for pure protein and pure pectin, suggesting that certain thermodynamic factors could contribute to the shift of pH_m with stoichiometric change. Furthermore, since the sigmoidal Boltzmann equation maybe a representative equation to describe the ordering parameter coupled with reversible gelation (Li et al., 2004; Navarro-Verdugo, Goycoolea, Romero-Melendez, Higuera-Ciapara, & Arguelles-Monal, 2011), it indicates that the pH_m could be a good ordering parameter to characterize the phase behavior associated with protein/polysaccharide complex coacervation, and the coacervation is somehow similar to physical gelation.

To further understand the physical nature behind pH_m, we attempt to locate pH_m using the concepts which assume that the system either has a minimum in interaction potential, or is ultimately charge neutralized. In the first case, we assume that there is a reversible equilibrium between protein/polysaccharide complex and their isolated forms. It can be expressed as $\alpha PRO + PS \rightleftharpoons PS\text{-}PRO_\alpha$, and $[PS\text{-}PRO_\alpha] = k_c\,[PRO][PS]$ with k_c the equilibrium constant. Then the interaction potential in the system can be written as

$$E = [PRO]E(\rho_{PRO}, \rho_{PRO}) + [PS]E(\rho_{PS}, \rho_{PS}) + [PRO - PS_\alpha]E(\rho_{PRO}, \rho_{PS}) \quad (6)$$

Here ρ_{PS} is the charge density (partial charges per unit mass) of polysaccharide, contributed from the dissociation of carboxyl group and has a maximum of $-0.69/m_{PS}$ (e.u./Da) according to the 31% esterification of the sample. ρ_{PRO} is the charge density of a BSA at a given pH, where the charges can be contributed from the dissociation of carboxyl group and the protonation of amide group. It can be contributed from either titratable residues (i.e., solvent accessible and charged residues) or all charged residues in the protein. The average molecular weight of pectin monomer m_{PS} is 181 Da, and the molecular weight of BSA is 66,172 Da. Since the electrostatic interaction dominates the final phase equilibrium, the pair-wise interaction can be modeled by the Derjaguin–Landau–Verwey–Overbeek (DLVO) potential (Russel, Saville, & Schowalter, 1989)

$$E(\rho_i, \rho_j) = \rho_i \rho_j \lambda_B \frac{e^{\sigma_i/\lambda_D}}{1+\sigma_i/\lambda_D} \frac{e^{\sigma_j/\lambda_D}}{1+\sigma_j/\lambda_D} \sum_r \frac{e^{-r/\lambda_D}}{r} \quad (7)$$

Here σ_i represents the radii of protein or polysaccharide bead. The $\sum()$ is the sum of electrostatic interaction in the distance ranging from $\sigma_i + \sigma_j$ to $\sigma_i + \sigma_j + 12\lambda_D$. To simplify the calculation by taking into account the effects of the protein to polysaccharide ratio on the interaction potential profile change, Eq. (6) can be rewritten as

$$E(\alpha, \mathrm{pH}, k_c) = \alpha E(\rho_{PRO}, \rho_{PRO}) + E(\rho_{PS}, \rho_{PS}) + k_c \alpha E(\rho_{PRO}, \rho_{PS}) \quad (8)$$

Therefore, at a given α (or f_{PS}) and a fixed k_c, the potential $E(\alpha, \mathrm{pH}, k_c)$ has a minimum at the critical pH. We plot the critical pH values against different equilibrium constants k_c, and the results are shown in Fig. 4. The critical pH shifts to a lower value as f_{PS} increases or k_c decreases. The best matched critical pH region based on pH_m changes from 4.24 to 1.89 when k_c is between 50 and 100 with the mass ratio of BSA to pectin in the same experimental setting range. It indicates the association proneness of BSA and pectin is quite high. The critical pH variation range is slightly narrower than the experimental observation, which suggests more detail should be taken into consideration for better prediction of the critical pH values. Nevertheless, the summation of DLVO potential qualitatively represents the shift of pH_m to a lower value as the fraction of pectin increases, by considering either all charged residues or only titratable residues.

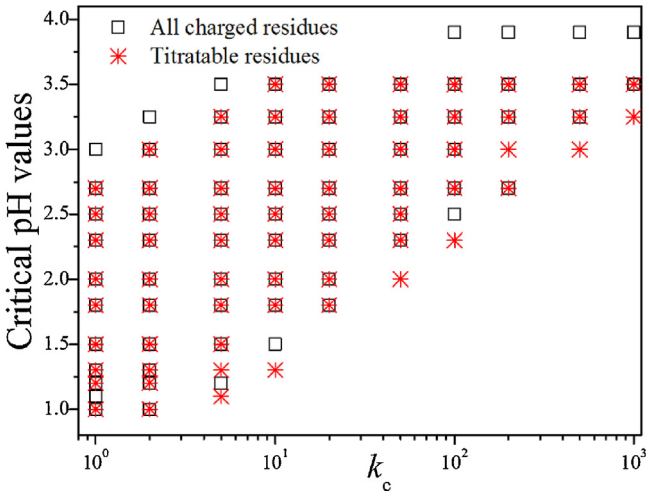

Fig. 4. The critical pH values which corresponding to the minimum DLVO potential at given mass fraction of polysaccharide were plotted against the equilibrium constants.

As for the second case, a number of reports have indicated that the complex coacervation is a result of charge neutralization (Antonov et al., 2010; Mekhloufi, Sanchez, Renard, Guillemin, & Hardy, 2005; Sanchez et al., 2002; Weinbreck, Nieuwenhuijse, Robijn, & de Kruif, 2003; Xu et al., 2011). In this system, at pH_m, the mixtures should have the least net charge. To verify this point, we calculated the net charge density in the mixture, ρ_{SYS} (in unit of e.u./Da) through

$$\rho_{SYS} = \rho_{PS} + \alpha\rho_{PRO} \quad (9)$$

ρ_{SYS} as a function of pH and f_{PS}, in consideration of all charged or titratable residues, and then merge the pH_m values were shown in Fig. 5. It can be seen that at pH_m, all mixtures are slightly positively charged. In the consideration of charge neutralization between titratable residues and PS chains, all pH_m points are located in very low net charge region with less than 1.0×10^{-3} e.u./Da. Whereas in the consideration of charge neutralization between all charged residues and PS chains, the net charge of the mixture has a higher value ($>1.2 \times 10^{-3}$ e.u./Da), except when PS is largely in excess, the net charge falls to low net charge density again. This result clearly shows that the titratable residues rather than all charged residues participated in the charge neutralization during protein/polysaccharide complex coacervation.

3.3. Monte Carlo simulation

Monte Carlo simulation on the BSA/pectin mixture system was also used to reveal more details. Typical snapshots of simulation configurations under thermodynamic equilibrium were shown in Fig. 6. The largest aggregate in each snapshot was identified by setting $\Gamma = -2$. The pH range is from 2.0 to 5.5, which covers the pH window for complex coacervation in BSA/pectin mixtures. In all situations, protein–PS association is always the major scenario in complex formation as well as subsequent aggregation for complex coacervation. At the different protein/PS ratios, complex coacervate can also be formed through other pathways. For example, in the ratio of 5:1 samples, protein is in excess, aggregates can be enlarged through the packing of proteins; in the ratio of 1:5 samples, PS is in excess, coacervation can be promoted through the entanglement of PS chains; while in the ratio of 1:1 samples, both the packing of proteins and the entanglement of PS chains can facilitate coacervation. In the former two cases, small amount of

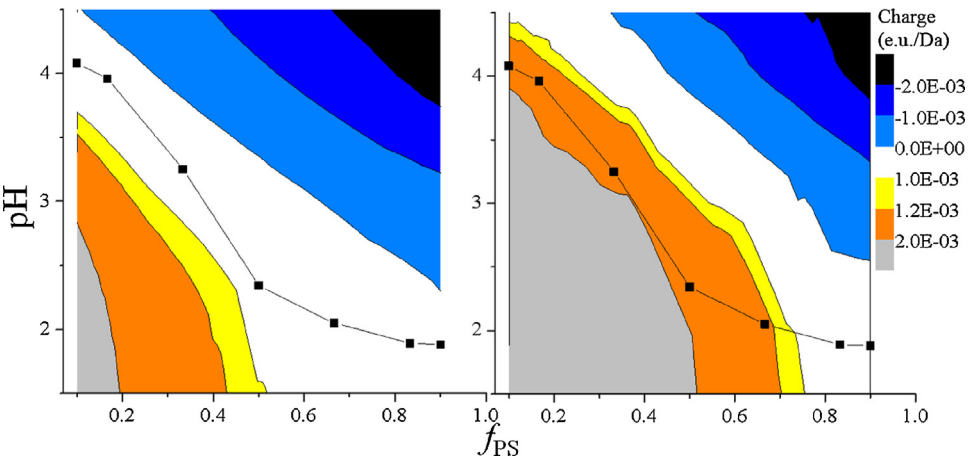

Fig. 5. Charge neutralization of BSA and pectin mixture in consideration of titratable residues in protein surface (left) and all chargeable residues in BSA (right). The NaCl concentration is fixed at 0.1 M.

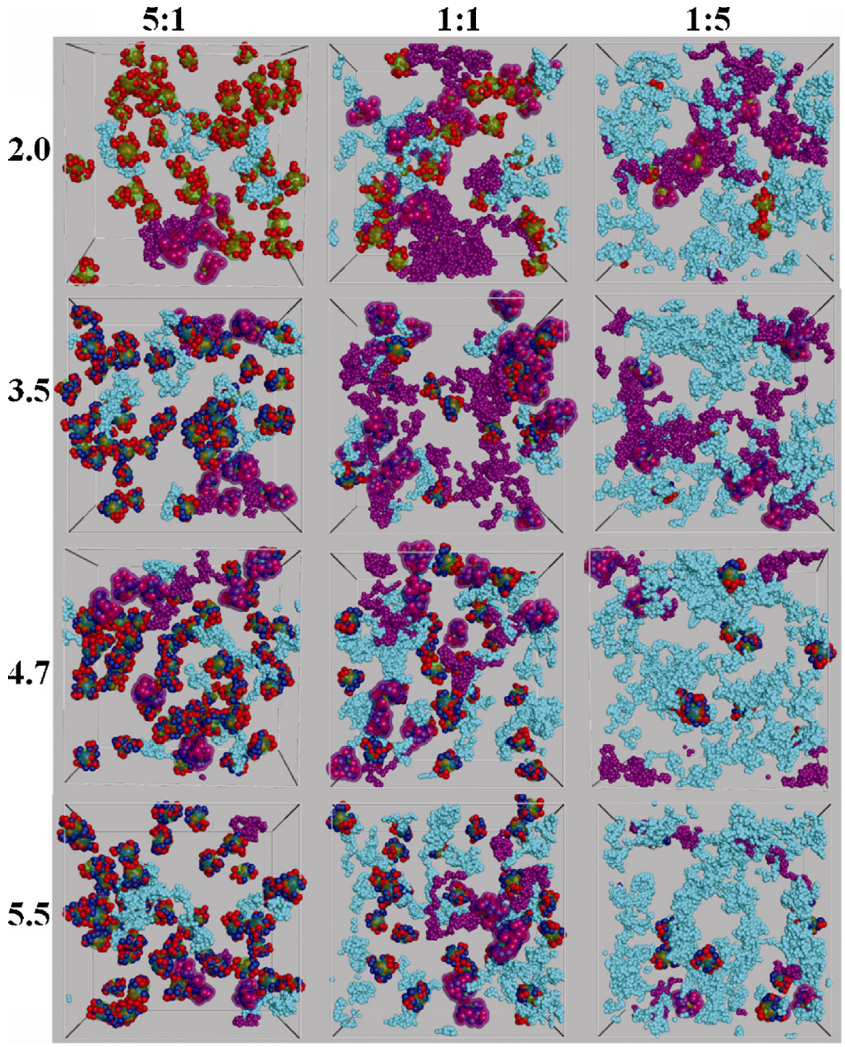

Fig. 6. Snapshots of simulation configurations under thermodynamic equilibrium. Each column shows configurations at different PRO/PS ratio of 5:1, 1:1 and 1:5, and each row presents configurations from pH 2.0, 3.5, 4.7 and 5.5. In each snapshot, gray lines show the periodic boundaries, cyan beads, red/blue spheres, and green bulbs represent PS beads, positive/negative charge patches and the excluded volume of proteins, respectively. The purple colored out the largest aggregate in each snapshot. (For interpretation of the references to color in this figure legend, the reader is referred to the web version of the article.)

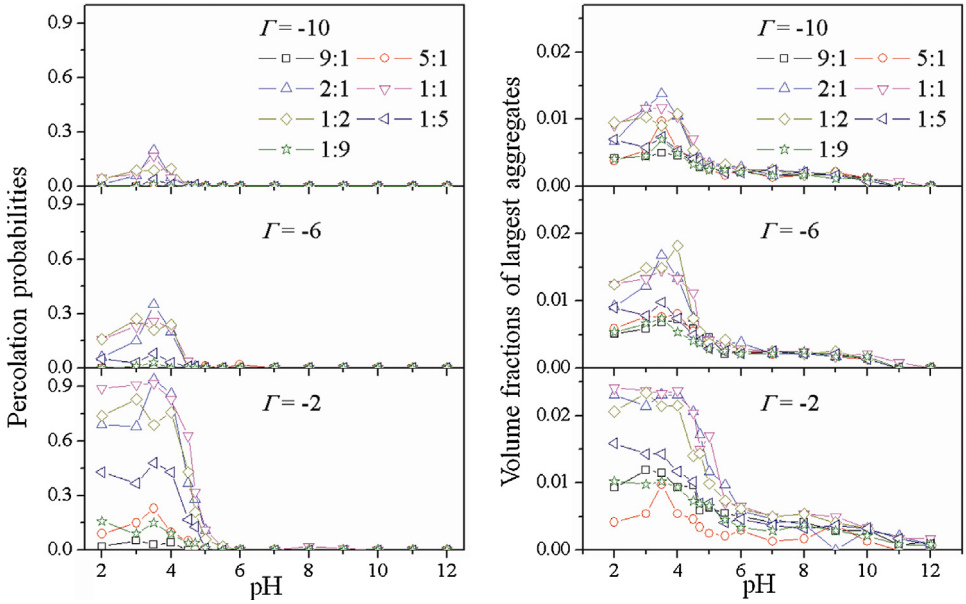

Fig. 7. Percolation probability (left) and the volume fraction of the largest aggregate (right) as a function of the protein/polysaccharide ratio and pH at different intermolecular association strength cutoffs.

molecules were trapped in the largest aggregate, while in the last case, a large amount of molecules can be enclosed in the largest aggregate because the mixture is highly charge-neutralized. Similarly, significantly more molecules are entrapped in the largest aggregation also can be observed when pH approaches to 3.5.

We then calculated the percolation probability (i.e., the number of percolated samples out of the 100 configurations under thermodynamic equilibrium) and the size (i.e., the volume fraction in simulation box) of the largest aggregate using the method described before (Li et al., 2012). The results with intermolecular attraction thresholds of −2, −6 and $-10k_BT$ were presented in Fig. 6. When Γ was adjusted to represent aggregate with stronger intermolecular association, both the percolation probability and the size of the largest aggregate decreased. Upon decreasing pH, the initialization of complexation took place at high pH (e.g., ~11.0), while complex coacervation occurred at relatively low pH (e.g., ~5.0). These two pH values are similar to the pH_c and the pH_φ as reported in literatures (Weinbreck, de Vries, Schrooyen, & de Kruif, 2003; Xu et al., 2011). However, the difference between them is prominent, the simulation shows complex in much broader pH range, larger than that from experimental observation, suggesting that the initial binding behavior of protein/polysaccharide may not cause visible turbidity increase. Furthermore, the positively charged patches in protein contained arginine and lysine, both have high p*K*a values of 12.0 and 10.5 respectively, still bring some positive charge at high pH. It can attract pectin chains with negative charges to form complex. The onsets of the sharp increase of the percolation probabilities and the size of the largest aggregates are quite consistent, and they are very close to the turbidimetric titration measurement. The shapes of pH-dependent profiles also agree well with experimental observation, except for the ratio-dependant variation in pH_m. The pH_m from simulation is around 3.5, a value close to most of the pH_m values from turbidimetric titration measurements, but failed to represent the ratio dependence. This failure may be contributed from multiple reasons, such as charge induced persistence length chain in pectin chains is not considered in current freely jointed chain model, charge regulation during complexation (Boral & Bohidar, 2010; da Silva & Jönsson, 2009; Lund & Jönsson, 2005) and contour-ion condensation (Turgeon, Schmitt, & Sanchez, 2007) are not counted. Future simulation works taking consideration of persistence length of polysaccharide chains and explicit solvent to address their contributions are undergoing. Nevertheless, the highly consistent results of the phase boundaries from Monte Carlo simulation to the turbidimetric titration experiment suggest that the implement of percolation concepts and the coarse-grained model used in this work is capable to simulate key features of the complex coacervation in BSA/pectin mixtures (Fig. 7).

Furthermore, since electrostatic interaction usually dominates complex coacervation in protein/polysaccharide mixtures, the binding sites in proteins which are bound to charged polysaccharides should be in charge patches. It should be noted that the binding site in a protein may contain multiple residues with different properties, we limited it to charge patches because electrostatic interaction dominated the binding behavior in this system. To make clear how the features of charge patches contribute to their binding affinity, we calculated the average electrostatic interaction contributed by each charge patch, and plotted it against pH and the partial charge (Fig. 8). Overall, the charge patches with more charges have larger intermolecular electrostatic interactions. The strongest binding occurs at pH from 4.0 to 6.0, and the strongest repulsion occurs on those patches brought large amount of negative charges. Among the three ratios shown, protein charge patches have the strongest binding affinity in the ratio of 1:1 samples. At all ratios and pH values, the charge patches with the strongest binding affinity to PS chains through electrostatic attraction are convergent to the largest positive change patch, the one in red color as illustrated in Fig. 1. Therefore, the largest positive charge patches are the most important binding sites for complex coacervation in BSA/pectin mixtures through electrostatic attraction.

4. Discussions

Through the comparison of the pH windows in which complex coacervation takes place in BSA/pectin mixture, both turbidimetric titration and Monte Carlo simulation present almost identical phase boundaries. When the ratio of BSA to pectin increases, the experimental results suggest that a maximum turbidity of the mixture appears at the ratio between 5:1 and 2:1, while the simulation results present that it is between 2:1 and 1:2. This difference suggests that either the coarse grained model or the potentials guiding the simulation need further improvement to replicate all details of complex coacervation in protein/polysaccharide mixtures. Factors

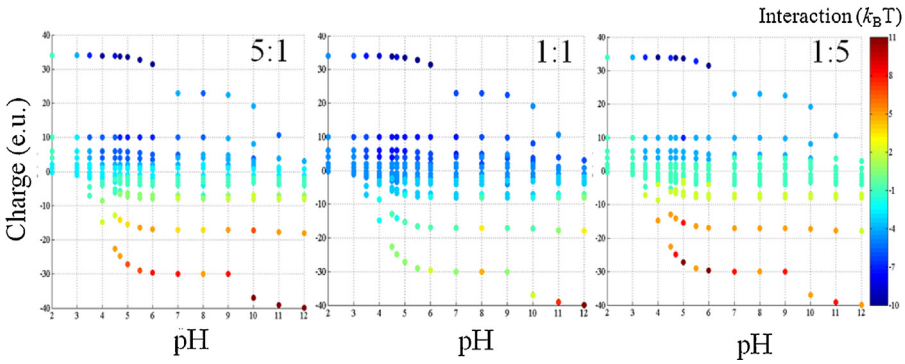

Fig. 8. Distribution of electrostatic interactions of charge patches in protein surface at different pHs and ratios. The colors from blue to red show the electrostatic interactions from strong attraction to strong repulsion. (For interpretation of the references to color in this figure legend, the reader is referred to the web version of the article.)

such as explicit solvent in the model to consider the condensation effect (Seijo, Ulrich, Filella, Buffle, & Stoll, 2009) and the regulation of charges (Seijo, Ulrich, Filella, Buffle, & Stoll, 2008; Ulrich, Seijo, Laguecir, & Stoll, 2006) during complexation, and charge induced conformation change of pectin chains may allow the observation of the pH_m shift with ratio. Furthermore, in the association of protein and PS chains, other interactions, such as hydrophobic interaction and depletion potential may also play non-negligible roles. The difference in the ratio may also come from the different contributions to complex coacervation in turbidimetric titration experiments and in simulations. In turbidimetric titration experiment, as shown in Fig. 2, the association of BSA has a large contribution in increasing turbidity than pectin. In simulation, we applied the concepts from geometric percolation to identify complex coacervate, where polysaccharide chains ($R_g \sim 57$ Å) have a larger contribution than protein (R_g 30.0 Å) in enlarging the complex domain. The relatively lower contribution of proteins in simulation resulted in the optimum ratio of BSA/pectin complex coacervation to be lower for simulation than the titration experiments. Overall, the matched pH windows of complex coacervation strongly suggested that the simulation had grasped the major feature of complex coacervation. The simulation also suggests that the intermolecular association strength is at several k_BT, a typically strength in soft condense matter which represents the reversible association under physical environmental perturbations (Zaccarelli, 2007) and the strength of ionic bond with low salt (Spruijt, van den Berg, Stuart, & van der Gucht, 2012).

The existence of pH_m reported here may also widely exist during complex coacervation in other protein/polysaccharide mixtures, and can be experimentally observed as long as the total biopolymer concentration is in a proper range. The occurrence of pH_m can be easily understood based on previous reports by Gummel et al. (2008) and Zhang and Shklovskii (2004), where complex cores were ultimately charge neutralized. The isoelectric complex cores could further aggregate widely, resulting in a high turbidity. The ratio dependence of pH_m can be described using sigmoidal Boltzmann equation, suggesting that the ratio can be an efficient factor to monitor the preparation of complex coacervate. The attempt to interpret pH_m using the minimization of interaction potential revealed that the equilibrium in the complex coacervation shifted as the protein to polysaccharide ratio changed. By taking into account of charge neutralization, pH_m was found to locate in the region which had very small net charge by the summation of partial charges brought by titratable residues and polysaccharide chains. The simulation results also suggested a constant pH_m value at pH 3.5, which was located in the charge neutralization region and was insensitive to the ratio change. This critical pH value has been reported as the optimum entrapment condition for whey protein isolate/pectin complexes (Bedie et al., 2008). Meanwhile, the simulation results also suggest that the aggregates reach the largest sizes at pH_m, which is in agreement with the titration experiments.

Finally, we found that the strongest electrostatic interaction occurred when the charge patches contained the highest amount of positive charges. In reality, the real binding site in a protein is also dominated by its accessibility to PS chains. Thus, we calculated the total interaction energy (using Eq. (1)) contributed from each patch. The patches with the strongest attractive interaction in all pH values and under the same BSA to pectin ratio were summarized in Table S2 (see supplementary information). For electrostatic interaction, the largest positive charge patch (patch I) is always the strongest electrostatic interaction contributor, but is not always the most energy favorable binding site in the presence of van der Waals potential and the excluded volume effect of charge patches. Instead, there is a tradeoff between electrostatic attraction and excluded repulsion, and the most important binding site in proteins varied in 5 non-identical patches (patch II is actually a subset of patch I) at various pH values and ratios. As the strongest attractive charge patch, patch I is quite conservative in protein-rich mixtures and in binding to other proteins at low pH region. While patches from II to VI became the most important binding sites in the mixtures where the polysaccharide turned out to be the major component, their binding affinity with PS chains dominated the attractive interactions of charge patches. This result suggests that the binding sites of BSA may not be determined purely based on the anisotropic distribution of charged residues, a conventional way to identify binding sites of BSA as reported in literatures (Antonov et al., 2010; Grymonpre et al., 2001).

5. Conclusions

In this work, we used a combination of turbidimetric titration, sigmoidal Boltzmann equation and Monte Carlo simulation to understand the complex coacervation in protein and anionic polysaccharide mixtures. The effects of pH and the ratio of protein to polysaccharide on intermolecular association and complex coacervation, interactions from charge patches and the distribution of binding sites were investigated. The coarse grained Monte Carlo simulation combined with percolation concepts can present the identical phase boundary of complex coacervation in serum albumin and pectin mixtures as that determined from titration experiments. The condition for the maximum turbidity in the mixtures was found to be associated with charge neutralization of titratable residues and polysaccharide chains. We also identified the most important binding sites in protein responsible for non-selective electrostatic attraction and the binding sites accessible for polysaccharide chains. The approach introduced in this work is applicable to other protein/polysaccharide systems, and provides a

way to better understand the complex coacervation in biopolymer complex fluids.

Acknowledgements

This work was supported by Department of Agriculture National Research Initiative (#2009-35603-05071). We thank Dr. David A. Joiner at Kean University to support the computational resource for this work – funded by National Science Foundation project OCI-0722790.

Appendix A. Supplementary data

Supplementary material related to this article can be found, in the online version, at http://dx.doi.org/10.1016/j.carbpol.2013.09.056.

References

Antonov, M., Mazzawi, M., & Dubin, P. L. (2010). Entering and exiting the protein–polyelectrolyte coacervate phase via nonmonotonic salt dependence of critical conditions. *Biomacromolecules*, *11*(1), 51–59.

Bedie, G. K., Turgeon, S. L., & Makhlouf, J. (2008). Formation of native whey protein isolate-low methoxyl pectin complexes as a matrix for hydro-soluble food ingredient entrapment in acidic foods. *Food Hydrocolloids*, *22*(5), 836–844.

Bendedouch, D., & Chen, S. H. (1983). Structure and interparticle interactions of bovine serum albumin in solution studied by small-angle neutron scattering. *Journal of Physical Chemistry*, *87*, 1473–1477.

Bohidar, H., Dubin, P. L., Majhi, P. R., Tribet, C., & Jaeger, W. (2005). Effects of protein–polyelectrolyte affinity and polyelectrolyte molecular weight on dynamic properties of bovine serum albumin-poly(diallyldimethylammonium chloride) coacervates. *Biomacromolecules*, *6*(3), 1573–1585.

Boral, S., & Bohidar, H. B. (2010). Effect of ionic strength on surface-selective patch binding-induced phase separation and coacervation in similarly charged gelatin-agar molecular systems. *Journal of Physical Chemistry B*, *114*(37), 12027–12035.

Brzozowska, A. M., de Keizer, A., Norde, W., Detrembleur, C., & Stuart, M. A. C. (2010). Grafted block complex coacervate core micelles and their effect on protein adsorption on silica and polystyrene. *Colloid and Polymer Science*, *288*(10–11), 1081–1095.

Brzozowska, A. M., Zhang, Q., de Keizer, A., Norde, W., & Stuart, M. A. C. (2010). Reduction of protein adsorption on silica and polysulfone surfaces coated with complex coacervate core micelles with poly(vinyl alcohol) as a neutral brush forming block. *Colloids and Surfaces A*, *368*(1–3), 96–104.

Burova, T. V., Grinberg, N. V., Golubeva, I. A., Mashkevich, A. Y., Grinberg, V. Y., & Tolstoguzov, V. B. (1999). Flavour release in model bovine serum albumin/pectin/2-octanone systems. *Food Hydrocolloids*, *13*(1), 7–14.

Caruso, F., & Mohwald, H. (1999). Protein multilayer formation on colloids through a stepwise self-assembly technique. *Journal of the American Chemical Society*, *121*(25), 6039–6046.

Chodankar, S., Aswal, V. K., Kohlbrecher, J., Vavrin, R., & Wagh, A. G. (2008). Structural study of coacervation in protein–polyelectrolyte complexes. *Physical Review E*, *78*(3 Pt 1), 031913.

da Silva, F. L. B., & Jönsson, B. (2009). Polyelectrolyte–protein complexation driven by charge regulation. *Soft Matter*, *5*, 2862–2868.

de Kruif, C. G., Weinbreck, F., & de Vries, R. (2004). Complex coacervation of proteins and anionic polysaccharides. *Current Opinion in Colloid and Interface Science*, *9*(5), 340–349.

Del Carpio, C. A., Takahashi, Y., & Sasaki, S.-i. (1993). A new approach to the automatic identification of candidates for ligand receptor sites in proteins: (I) Search for pocket regions. *Journal of Molecular Graphics*, *11*(1), 23–29.

Dickinson, E. (1998). Stability and rheological implications of electrostatic milk protein–polysaccharide interactions. *Trends in Food Science & Technology*, *9*(10), 347–354.

Dickinson, E. (2003). Hydrocolloids at interfaces and the influence on the properties of dispersed systems. *Food Hydrocolloids*, *17*(1), 25–39.

Dickinson, E. (2008). Interfacial structure and stability of food emulsions as affected by protein–polysaccharide interactions. *Soft Matter*, *4*, 932–942.

Ge, S. R., Kojio, K., Takahara, A., & Kajiyama, T. (1998). Bovine serum albumin adsorption onto immobilized organotrichlorosilane surface: Influence of the phase separation on protein adsorption patterns. *Journal of Biomaterials Science, Polymer Edition*, *9*(2), 131–150.

Grymonpre, K. R., Staggemeier, B. A., Dubin, P. L., & Mattison, K. W. (2001). Identification by integrated computer modeling and light scattering studies of an electrostatic serum albumin-hyaluronic acid binding site. *Biomacromolecules*, *2*(2), 422–429.

Gummel, J., Boue, F., Clemens, D., & Cousin, F. (2008). Finite size and inner structure controlled by electrostatic screening in globular complexes of proteins and polyelectrolytes. *Soft Matter*, *4*(8), 1653–1664.

Jones, O. G., Decker, E. A., & McClements, D. J. (2010). Comparison of protein–polysaccharide nanoparticle fabrication methods: Impact of biopolymer complexation before or after particle formation. *Journal of Colloid and Interface Science*, *344*(1), 21–29.

Kabsch, W., & Sander, C. (1983). Dictionary of protein secondary structure: Pattern recognition of hydrogen-bonded and geometrical features. *Biopolymers*, *22*(12), 2577–2637.

Kalapathy, U., & Proctor, A. (2001). Effect of acid extraction and alcohol precipitation conditions on the yield and purity of soy hull pectin. *Food Chemistry*, *73*(4), 393–396.

Kayitmazer, A. B., Strand, S. P., Tribet, C., Jaeger, W., & Dubin, P. L. (2007). Effect of polyelectrolyte structure on protein–polyelectrolyte coacervates: Coacervates of bovine serum albumin with poly(diallyldimethylammonium chloride) versus chitosan. *Biomacromolecules*, *8*(11), 3568–3577.

Laos, K., Brownsey, G. J., & Ring, S. G. (2007). Interactions between furcellaran and the globular proteins bovine serum albumin and β-lactoglobulin. *Carbohydrate Polymers*, *67*(1), 116–123.

Li, Y., & Fang, J. (2010). Distance-dependent statistical potentials for discriminating thermophilic and mesophilic proteins. *Biochemical and Biophysical Research Communications*, *396*(3), 736–741.

Li, Y., Lee, J., Lal, J., An, L., & Huang, Q. (2008). Effects of pH on the interactions and conformation of bovine serum albumin: Comparison between chemical force microscopy and small-angle neutron scattering. *Journal of Physical Chemistry B*, *112*(12), 3797–3806.

Li, Y. J., Mattison, K. W., Dubin, P. L., Havel, H. A., & Edwards, S. L. (1996). Light scattering studies of the binding of bovine serum albumin to a cationic polyelectrolyte. *Biopolymers*, *38*(4), 527–533.

Li, Y., Shi, T., An, L., Lee, J., Wang, X., & Huang, Q. (2007). Effects of polar group saturation on physical gelation of amphiphilic polymer solutions. *Journal of Physical Chemistry B*, *111*(42), 12081–12087.

Li, Y., Shi, T., Huang, Q., & An, L. (2012). Monte Carlo simulation on complex and complex coacervation of protein and polysaccharide. *Journal of Physical Chemistry B*, *116*(10), 3045–3053.

Li, Y., Sun, Z., Shi, T., & An, L. (2004). Conformation studies on sol–gel transition in triblock copolymer solutions. *Journal of Chemical Physics*, *121*(2), 1133–1140.

Liu, S., Low, N. H., & Nickerson, M. T. (2010). Entrapment of flaxseed oil within gelatin-gum arabic capsules. *Journal of the American Oil Chemists Society*, *87*(7), 809–815.

Lund, M., & Jönsson, B. (2005). On the charge regulation of proteins. *Biochemistry*, *44*(15), 5722–5727.

Manning, G. S. (1969). Limiting laws and counterion condensation in polyelectrolyte solutions. I. Colligative properties. *Journal of Chemical Physics*, *51*(3), 924–933.

Marcelo, G., Saiz, E., & Tarazona, M. P. (2005). Unperturbed dimensions of Carrageenans in different salt solutions. *Biophysical Chemistry*, *113*(3), 201–208.

Marszalek, P. E., Li, H., Oberhauser, A. F., & Fernandez, J. M. (2002). Chair-boat transitions in single polysaccharide molecules observed with force-ramp AFM. *Proceedings of the National Academy of Sciences of the United States of America*, *99*(7), 4278–4283.

Mekhloufi, G., Sanchez, C., Renard, D., Guillemin, S., & Hardy, J. (2005). pH-induced structural transitions during complexation and coacervation of beta-lactoglobulin and acacia gum. *Langmuir*, *21*(1), 386–394.

Metropolis, N., Rosenbluth, A. W., Rosenbluth, M. N., Teller, A. H., & Teller, E. (1953). Equation of state calculations by fast computing machines. *Journal of Chemical Physics*, *21*(6), 1087–1092.

Navarro-Verdugo, A. L., Goycoolea, F. M., Romero-Melendez, G., Higuera-Ciapara, I., & Arguelles-Monal, W. (2011). A modified Boltzmann sigmoidal model for the phase transition of smart gels. *Soft Matter*, *7*(12), 5847–5853.

Norberg, J., & Nilsson, L. (2000). On the truncation of long-range electrostatic interactions in DNA. *Biophysical Journal*, *79*(3), 1537–1553.

Pace, C. N., Grimsley, G. R., & Scholtz, J. M. (2009). Protein ionizable groups: p*K* values and their contribution to protein stability and solubility. *Journal of Biological Chemistry*, *284*(20), 13285–13289.

Ru, Q., Wang, Y., Lee, J., Ding, Y., & Huang, Q. (2012). Turbidity and rheological properties of bovine serum albumin/pectin coacervates: Effect of salt concentration and initial protein/polysaccharide ratio. *Carbohydrate Polymers*, *88*(3), 838–846.

Russel, W. B., Saville, D. A., & Schowalter, W. R. (1989). *Colloidal dispersions*. Cambridge: Cambridge University Press.

Sanchez, C., Mekhloufi, G., Schmitt, C., Renard, D., Robert, P., Lehr, C. M., et al. (2002). Self-assembly of beta-lactoglobulin and acacia gum in aqueous solvent: Structure and phase-ordering kinetics. *Langmuir*, *18*(26), 10323–10333.

Schmidt, I., Cousin, F., Huchon, C., Boue, F., & Axelos, M. A. (2009). Spatial structure and composition of polysaccharide–protein complexes from small angle neutron scattering. *Biomacromolecules*, *10*(6), 1346–1357.

Schmitt, C., Sanchez, C., Desobry-Banon, S., & Hardy, J. (1998). Structure and technofunctional properties of protein–polysaccharide complexes: A review. *Critical Reviews in Food Science and Nutrition*, *38*(8), 689–753.

Seijo, M., Ulrich, S., Filella, M., Buffle, J., & Stoll, S. (2008). Modeling the surface charge evolution of spherical nanoparticles by considering dielectric discontinuity effects at the solid/electrolyte solution interface. *Journal of Colloid and Interface Science*, *322*(2), 660–668.

Seijo, M., Ulrich, S., Filella, M., Buffle, J., & Stoll, S. (2009). Modeling the adsorption and coagulation of fulvic acids on colloids by brownian dynamics simulations. *Environmental Science & Technology*, *43*(19), 7265–7269.

Seyrek, E., Dubin, P. L., Tribet, C., & Gamble, E. A. (2003). Ionic strength dependence of protein–polyelectrolyte interactions. *Biomacromolecules*, *4*(2), 273–282.

Sinha, R., Kundrotas, P. J., & Vakser, I. A. (2012). Protein docking by the interface structure similarity: How much structure is needed? *PLoS ONE*, *7*(2), e31349.

Spruijt, E., van den Berg, S. A., Stuart, M. A. C., & van der Gucht, J. (2012). Direct measurement of the strength of single ionic bonds between hydrated charges. *Acs Nano*, *6*(6), 5297–5303.

Tanford, C., & Kirkwood, J. G. (1957). Theory of protein titration curves. 1. General equations for impenettrable spheres. *Journal of the American Chemical Society*, *79*(20), 5333–5339.

Toh, Y. C., Ho, S. T., Zhou, Y., Hutmacher, D. W., & Yu, H. (2005). Application of a polyelectrolyte complex coacervation method to improve seeding efficiency of bone marrow stromal cells in a 3D culture system. *Biomaterials*, *26*(19), 4149–4160.

Tolstoguzov, V. (2003). Some thermodynamic considerations in food formulation. *Food Hydrocolloids*, *17*(1), 1–23.

Turgeon, S. L., Schmitt, C., & Sanchez, C. (2007). Protein–polysaccharide complexes and coacervates. *Current Opinion in Colloid and Interface Science*, *12*(4–5), 166–178.

Ulrich, S., Seijo, M., Laguecir, A., & Stoll, S. (2006). Nanoparticle adsorption on a weak polyelectrolyte. Stiffness, pH, charge mobility, and ionic concentration effects investigated by Monte Carlo simulations. *Journal of Physical Chemistry B*, *110*(42), 20954–20964.

Wang, X. Y., Ho, C. T., & Huang, Q. R. (2007). Investigation of adsorption behavior of (−)-epigallocatechin gallate on bovine serum albumin surface using quartz crystal microbalance with dissipation monitoring. *Journal of Agricultural and Food Chemistry*, *55*(13), 4987–4992.

Wang, X. Y., Lee, J. Y., Wang, Y. W., & Huang, Q. R. (2007). Composition and rheological properties of beta-lactoglobulin/pectin coacervates: Effects of salt concentration and initial protein/polysaccharide ratio. *Biomacromolecules*, *8*(3), 992–997.

Wang, X., Wang, Y.-W., Ruengruglikit, C., & Huang, Q. (2007). Effects of salt concentration on formation and dissociation of β-lactoglobulin/pectin complexes. *Journal of Agricultural and Food Chemistry*, *55*(25), 10432–10436.

Weinbreck, F., de Vries, R., Schrooyen, P., & de Kruif, C. G. (2003). Complex coacervation of whey proteins and gum arabic. *Biomacromolecules*, *4*(2), 293–303.

Weinbreck, F., Nieuwenhuijse, H., Robijn, G. W., & de Kruif, C. G. (2003). Complex formation of whey proteins: Exocellular polysaccharide EPS B40. *Langmuir*, *19*(22), 9404–9410.

Xia, J. L., Dubin, P. L., & Dautzenberg, H. (1993). Light-scattering, electrophoresis, and turbidimetry studies of bovine serum-albumin poly(dimethyldiallylammonium chloride) complex. *Langmuir*, *9*(8), 2015–2019.

Xu, Y., Mazzawi, M., Chen, K., Sun, L., & Dubin, P. L. (2011). Protein purification by polyelectrolyte coacervation: Influence of protein charge anisotropy on selectivity. *Biomacromolecules*, *12*(5), 1512–1522.

Zaccarelli, E. (2007). Colloidal gels: Equilibrium and non-equilibrium routes. *Journal of Physics: Condensed Matter*, *19*(32), 323101.

Zhang, R., & Shklovskii, B. I. (2004). Phase diagram of aggregation of oppositely charged colloids in salty water. *Physical Review E*, *69*(2), 021909.